Solution of Euler equations for unsteady flow problems using a central compact scheme

Abhishek Kundu[1*]

[1] *Department of Mechanical Engineering, Institute of Engineering & Management, Kolkata – 700091, West Bengal, India*

Email: abhishekkundu45@gmail.com

Abstract

We solve the Euler equations in one and two dimensions using a central compact scheme coupled with an AUSM$^+$ algorithm. The compact scheme is used in the form of a cell-face interpolation scheme to create the left- and right-states of the primitive variables required by the AUSM$^+$ based solver. We invoke a TVD limiter to locally apply smaller stencil low-order dissipative formulae near shocks. No extra high-order artificial dissipation is added to stabilize the computation. A number of one and two dimensional test cases has been solved to show the effectiveness of this approach.

Keywords: Euler equations; central compact scheme; AUSM$^+$; TVD limiter; shock capturing

1. Introduction

In a compact scheme, derivatives of a variable in a number of neighbouring cells are coupled together in an implicit equation to derive a high-order accurate formula. Compact schemes were suggested in the year 1972 for solving problems related to `high altitude motion of bodies' by A. I. Tolstykh [1,2]. A fourth-order compact differencing scheme derived by H.-O. Kreiss was applied for a number of problems including the driven cavity in 1975 [3]. The cited book by Tolstykh and the paper by Lele on compact schemes [4] shows that compact schemes can achieve very high accuracy in the wavenumber space for a given formal order of accuracy. The CUD-3 - one of the earliest known compact schemes used for fluid dynamic applications - is one such scheme which has a dispersion error that is very low for a third-order scheme [1]. This accuracy is very desirable when one computes small scale vortices. In compressible flow applications, one often needs to resolve such small scale structures in the presence of shock waves. A wide-stencil first derivative formula or a compact scheme that extends across a shock wave gives rise to wiggles in the solution - a phenomenon that can be handled if narrow-stencil and low-order dissipative schemes are applied locally near shocks. This has been done in the widely used JST scheme [5], where a fourth-derivative numerical dissipation is activated in smooth regions and shocks are handled by a second-derivative dissipation scheme, depending on a pressure based switch. This method has recently been applied to the OUCS class of upwind compact schemes [6]. This, however, would lead to loss of accuracy of the original OUCS2 scheme that offers sixth-derivative dissipation. Though the dispersion error of the original compact scheme will remain untouched, the extra dissipation at lower wavenumbers due to the fourth-derivative would be detrimental to the resolution of the smaller scale structures. A more commonly used method of attenuating high wavenumber excitations that are beyond

the resolving capacity of the compact scheme is the application of low-pass filters to smooth the conserved variables [7]. To improve the stability of the solver, such filtering procedures often need extra dissipation coming from implicit operators [8]. This extra dissipation, once again, would bring down the original resolving capacity of the high-accuracy compact scheme. The key issue with the application of filters is the fact that their action is applied everywhere, irrespective of the location of shocks, causing robustness problems unless covered by an additional source of dissipation. To improve the situation, this additional dissipation has recently been proposed in the form of `localized artificial diffusivity' [9]. In this method, artificial fluid transport coefficients are locally activated to capture discontinuities. This method has been primarily tested for compressible turbulent flows. Its performance for strong shock-vortex interaction cases is not well documented. A compact differencing based solver can robustly handle shocks if coupled with a WENO (weighted-essentially-non-oscillatory) class of scheme [10,11]. Though shock capturing improves, it has been noted that `the numerical solutions obtained with ENO/WENO schemes in smooth regions with moderately high field gradients are not very satisfactory' [12].

Our aim in this paper is to develop a method of solving the Euler equations for unsteady flow problems that will be both simple to implement and fairly accurate. Based on the above discussion, we look for possibilities to extend an existing AUSM$^+$ based explicit solver. One example of this kind of resolution enhancement is found in Ravichandran [13]. Here Murman- and Roe-type first-order numerical flux is `post-processed' by an upwind compact scheme to achieve third-order accuracy. No flux-limiter was used, and oscillatory behaviour of the solution near discontinuities was predicted. Another example is given by Jun *et al.* [14]. The authors obtained the left and right states at the cell-faces for flux evaluation by a fourth-order MUSCL polynomial, followed by calculation of the derivative from the available fluxes at the cell-faces by a central compact scheme. We differ from this approach in the fact that we do not use the central compact scheme for flux-derivative calculation, rather we use it in the role of the MUSCL polynomials. MUSCL polynomials are dissipative in nature, whereas the compact scheme we employ is central - without any inbuilt dissipation. To take care of sharp gradients, we use a TVD limiter and a third-order MUSCL scheme which activate when the central compact scheme is not selected by the limiting scheme. In smoother regions, when the compact scheme becomes active, it operates without any inbuilt dissipation - unlike the upwind-type compact schemes [15,16]. A four-stage Runge-Kutta scheme is used for time-integration and no filtering is performed on the conserved variables. A number of challenging test cases have been solved to prove the robustness and accuracy of the presented method.

2. Euler equations and AUSM$^+$ algorithm details

The Euler equations for compressible fluid flow are given by

$$\frac{\partial q}{\partial t} + \frac{\partial f}{\partial x} + \frac{\partial g}{\partial y} = 0 \qquad (1)$$

where $$q = \begin{pmatrix} \rho \\ \rho u \\ \rho v \\ \rho E \end{pmatrix}, \qquad f = \begin{pmatrix} \rho u \\ \rho u^2 + p \\ \rho uv \\ (\rho E + p)u \end{pmatrix}, \qquad g = \begin{pmatrix} \rho v \\ \rho uv \\ \rho v^2 + p \\ (\rho E + p)v \end{pmatrix}.$$

Here ρ is the gas density, p is the pressure and u, v are the velocity components in the x- and y-directions, respectively. Energy is given by $\rho E = \frac{p}{\gamma - 1} + \frac{1}{2}\rho\left(u^2 + v^2\right)$. In the AUSM$^+$ algorithm [17], the cell-face flux $f_{i+\frac{1}{2},j}$ for the x-momentum equation is written as

$$f_{i+\frac{1}{2},j} = a_{i+\frac{1}{2},j}\left[\frac{1}{2}m_{i+\frac{1}{2},j}\left(\Phi_L + \Phi_R\right) - \frac{1}{2}\Psi_{i+\frac{1}{2},j}\left(\Phi_R - \Phi_L\right)\right] + p_{i+\frac{1}{2},j} \tag{2}$$

For the other equations, the pressure term $p_{i+\frac{1}{2},j}$ will be absent. Here $m_{i+\frac{1}{2},j}$ is an interface Mach number and $a_{i+\frac{1}{2},j}$ is the interface speed of sound. In the original AUSM$^+$, $\Psi_{i+\frac{1}{2},j} = | m_{i+\frac{1}{2},j} |$. We use a modified version [18,19] in which

$$\Psi_{i+\frac{1}{2},j} = \frac{m^2{}_{i+\frac{1}{2},j} + \delta^2}{2\delta} \tag{3}$$

The above activates for $| m_{i+\frac{1}{2},j} | < \delta$ .This implies a non-zero dissipation coefficient of δ/2 as interface Mach number goes to zero. A value of δ = 0.1 has been used in our solver. Details of the AUSM$^+$ can be found in Liou [17], and will not be repeated here. The form of a numerical flux function as represented by Equation (2) is essential for describing the application of the central compact scheme. The Φ_L and Φ_R are the left and right states. In the x-momentum equation, for example, $\Phi_L = \rho_L u_L$. The left or right state of the primitive variables ρ and u are usually calculated by a MUSCL-type scheme, as suggested by Liou [17]. This is where we apply the compact scheme, as described next.

3. The central compact scheme and its properties

The central compact scheme that we employ here is given by

$$\alpha u'_{j-1} + u'_j + \alpha u'_{j+1} = \frac{a\left(u_{j+1} - u_{j-1}\right)}{h} + \frac{b\left(u_{j+2} - u_{j-2}\right)}{h} \tag{4}$$

It is possible to derive a sixth-order central scheme from the above. We will derive a scheme with fourth-order accuracy, for which $b = \frac{4\alpha - 1}{12}$, $a = \frac{\alpha + 2}{3}$. Note that if we choose α = 1/4, a fourth-order central scheme results with reduced stencil size, since b = 0. Our choice for α is α = 0.373092. This result is high accuracy in the wavenumber space, as shown in Figure 1. To apply this to calculate the cell-face values of the primitive variables, we write Equation (4) as

$$\alpha u_{j-\frac{1}{2}} + u_{j+\frac{1}{2}} + \alpha u_{j+\frac{3}{2}} = c\left(u_j + u_{j+1}\right) + b\left(u_{j-1} + u_{j+2}\right) \tag{5}$$

Here the new coefficient c = $\frac{8\alpha + 7}{12}$. Equation (5) can be used to calculate both the left and right states of u at $j + \frac{1}{2}$. This would introduce zero numerical dissipation, but near shocks where low-order dissipation is required, the limiter does not select this scheme and low-order dissipation comes from alternative small-stencil formulae. This scheme will be referred to as the COMPCS1 (Compact Central Scheme). A single boundary closure scheme is needed, and this is given by

$$u_{j+\frac{1}{2}} + \frac{6}{10} u_{j+\frac{3}{2}} = \frac{3u_j + 12u_{j+1} + u_{j+2}}{10} \tag{6}$$

A similar formula will be required at the other end of the domain.

4. The limiter

For any scheme, we can write the interpolated left state at the cell-face as

$$u_{j+\frac{1}{2},L} = u_j + \frac{1}{2}\beta_L\left(u_j - u_{j-1}\right) \tag{7}$$

A TVD limiter [20] can be used to limit the above as

$$u_{j+\frac{1}{2},L} = u_j + \frac{1}{2}\max\left(0, \min\left(2, 2\frac{\Delta u_{j+\frac{1}{2}}}{\Delta u_{j-\frac{1}{2}}}, \beta_L\right)\right)\left(u_j - u_{j-1}\right) \tag{8}$$

In Equation (8), $\Delta u_{j+\frac{1}{2}} = u_{j+1} - u_j$ and $\Delta u_{j-\frac{1}{2}} = u_j - u_{j-1}$. Let us write $r_L = \frac{\Delta u_{j+\frac{1}{2}}}{\Delta u_{j-\frac{1}{2}}}$. The function $\min\left(2, 2r_L, \beta_L\right)$ checks whether the numerical scheme (that corresponds to the β_L) lies within Harten's TVD region [21]. It is possible to use Equation (8) for the compact scheme alone, or in combination with other schemes. We use it together with the following explicit interpolation scheme:

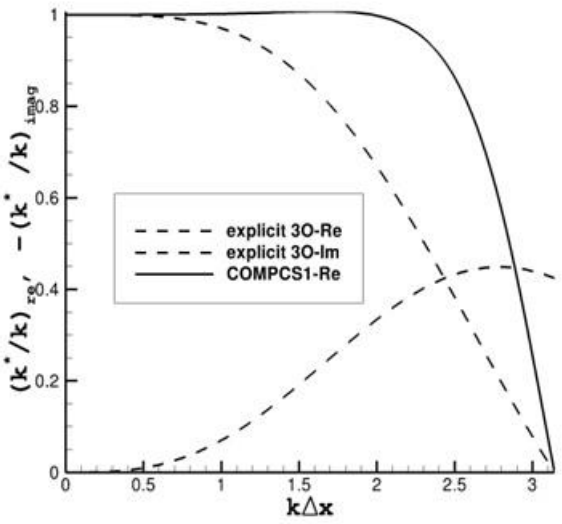

FIG 1. . Real and imaginary components of the modified wavenumber for the central compact scheme (COMPCS1) and the third order explicit scheme.

$$u_{j+\frac{1}{2},L} = \frac{2u_{j+1} + 5u_j - u_{j-1}}{6} \qquad (9)$$

Thus if the compact scheme does not lie within the TVD region, we check whether the scheme given by Equation (9) does. If it does, this explicit scheme is utilized. Otherwise the limiter selects a scheme from the remaining three possibilities from $\max(0, \min(2, 2r_L))$.

5. Results and discussion

In this section, a number of test cases in one and two dimensions will be solved using the COMPCS1 in combination with the limiting strategy presented above. Time stepping is performed by a four-stage Runge-Kutta scheme [22]. Given the governing equation in the form $\frac{du}{dt} = f(t,u)$, the time stepping scheme can be written as:

$$du^{(k)} = A^{(k)} du^{(k-1)} + \Delta t f\left(u^{(k-1)}\right)$$
$$u^{(k)} = u^{(k-1)} + B^{(k)} du^{(k)}$$

In the above, k = 1,4; $u^{(0)} = u^{(n)}$, $u^{(4)} = u^{(n+1)}$. The constants $A^{(k)}$ and $B^{(k)}$ are given by $A^{(1)} = 0$, $A^{(2)} = -5/9$, $A^{(3)} = -1$, $A^{(4)} = -33/25$; $B^{(1)} = 1/9$, $B^{(2)} = 3/4$, $B^{(3)} = 2/5$, $B^{(4)} = 5/4$.

5.1 Shu-Osher problem: Mach 3 shock interacting with a density wave

We solve the 1-D Euler equations in a domain $-5 \leq x \leq 5$. The initial condition is given by

$$(\rho, u, p) = \begin{cases} (3.857143, 2.629369, 10.333333), x < -4 \\ (1 + 0.2\sin(5x), 0, 1), x \geq -4 \end{cases} \quad (10)$$

This problem is chosen to show the effectiveness of the compact scheme in smoother regions. 400 cells are taken in the domain and the Euler equations are solved with a CFL of 0.1. Figure 2 shows the density at t = 1.8. The reference solution is computed on a grid of 4000 cells using a ninth-order explicit scheme. From the figure, it is evident that the COMPCS1 resolves the density fluctuations much better than the explicit third-order scheme.

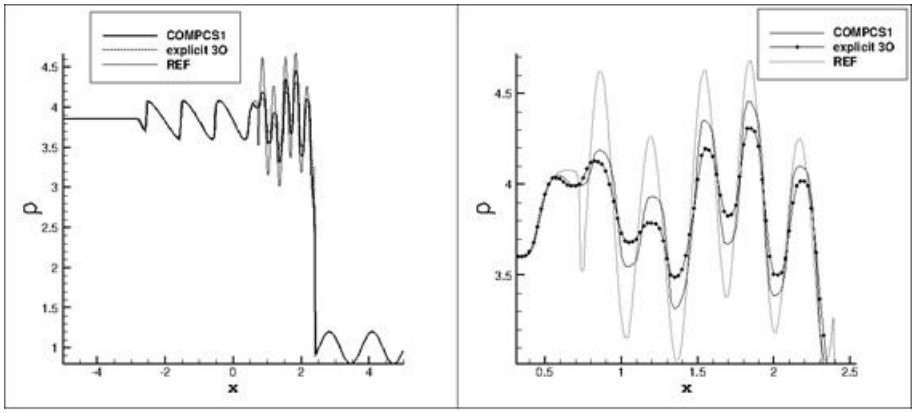

FIG 2. . The Shu-Osher problem of shock-density-wave interaction. Left frame: full domain, right frame: zoomed view of the fluctuating density at t = 1.8. CFL =0.1. Grid size: 400 cells.

5.2 Shu-Osher problem: interacting blast waves

For this problem, the initial conditions are given by $\rho = 1$, $u = 0$ everywhere in the domain between $0 \leq x \leq 1$. $p = 1000$ for $x < 0.1$; $p = 0.01$ for $0.1 \leq x < 0.9$; $p = 100$ for $x \geq 0.9$. Reflecting boundary conditions are applied at the ends. Figure 3 shows the results at t= 0.038. From the figure we note that the compact scheme results in sharper shock resolution. Only the density peak close to x = 0.8 is captured better by the

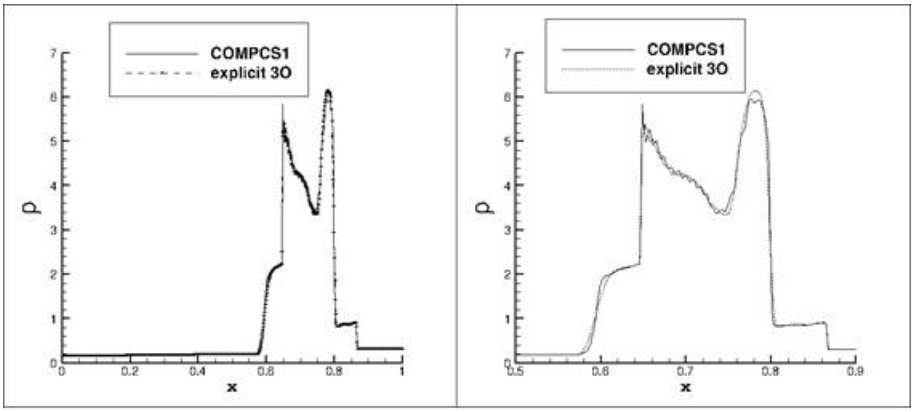

FIG 3. . Interacting blast wave: density at t = 0.038. Run with CFL = 0.1. Left frame: full domain; right frame: zoomed view. Grid size: 800 cells.

third-order explicit scheme. This problem is not ideal for high resolution compact schemes, which are meant for capturing smoother regions away from the discontinuities. This problem was chosen to check whether the limiter is functioning in the intended manner. These two problems show that the compact scheme-limiter combination is working effectively. We now move on to three problems in two dimensions where moving shocks, vortices and slip lines are present.

5.3 Shock diffraction at a corner

We solve the 2-D Euler equations in a domain $[x, y] \in [0,1] \times [0,1]$. We set a reflecting boundary condition at the bottom wall and the lower half part of the left wall. Top and right walls have artificial absorbing boundary condition [23]. The initial conditions inside the whole domain are u = v = 0, p = 1 and $\rho = 1$. At the inflow at the top half of the left wall p = 3 and the flow angle is $\pi/10$. This problem has features of the Schardin's problem [24,25], but it is much easier to set-up. In Figure 4 we display the numerical

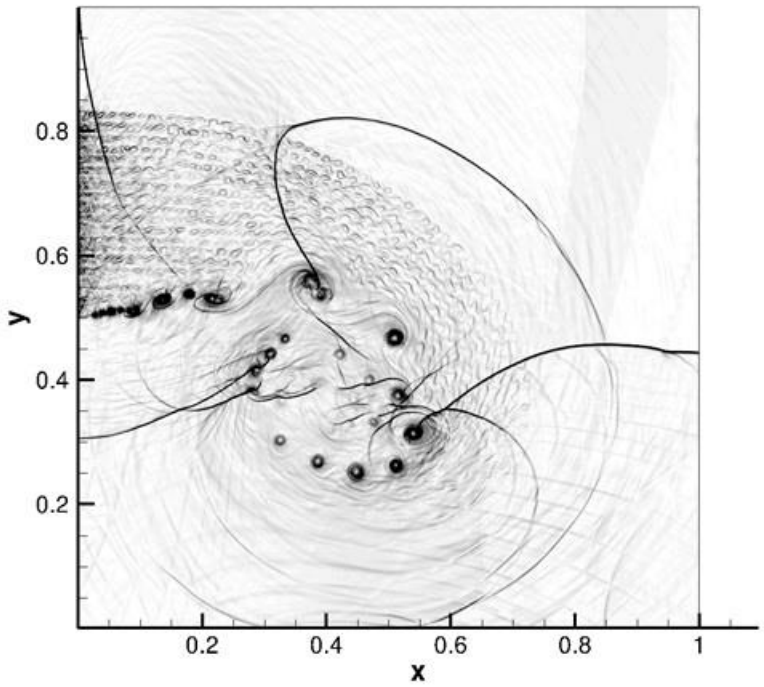

FIG 4 . Shock diffraction around a corner using the COMPCS1. Numerical schlieren at t = 1 with a $\Delta t = 10^{-4}$. Grid size: 1000×1000; RK four-stage time stepping. Forty contours from 1 to 40 have been plotted

schlieren at t = 1. At this point of time the initial shock wave that diffracts around the corner at the middle of the left wall has already reflected from the centreline. Diverging acoustic waves can be noticed attached to the small-scale vortices as it occurs in the Schardin's problem. An important feature that has been captured rather well is the series of small-scale rolled-up vortices from the inflow spiralling toward the core of the primary vortex. The high spectral accuracy of the COMPCS1 makes it possible to capture these small-scale structures right at the place where they are supposed to originate. On their way to the

central part of the main vortex they interact with the reflected shocks and acoustic waves. Correct representation of this shock-vortex interaction process depends on the resolution of the initial roll-up of the vortices near the inflow - and this is where the low dispersion error of the scheme is useful.

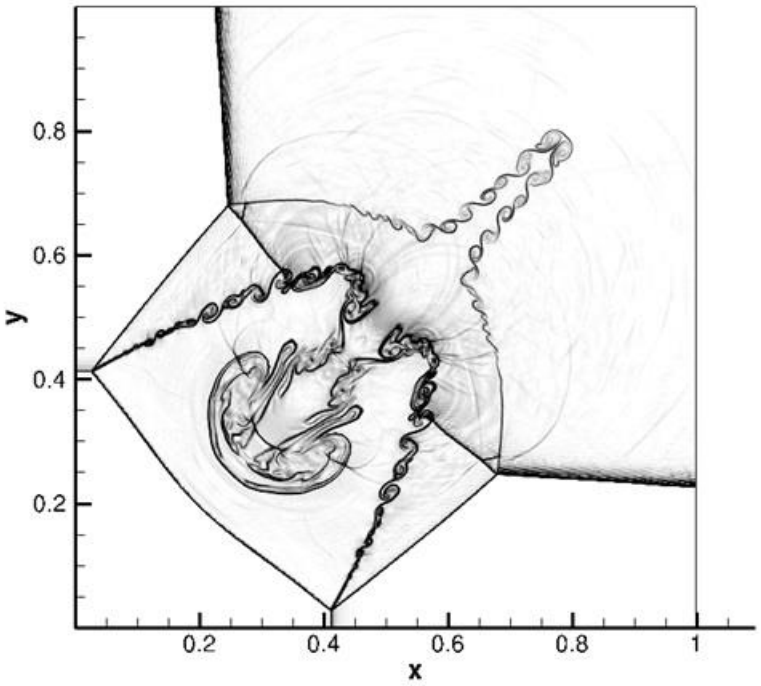

FIG 5. Four-shocks problem using the COMPCS1. Numerical schlieren at t = 0.8 with a CFL of 0.5. Grid size: 1000×1000; RK four-stage time stepping. Forty contours from 1 to 40 have been plotted.

5.4 Shock diffraction at a corner

This problem is taken from Schulz-Rinne *et al.* [26]. The domain is the same as before: $[x, y] \in [0,1] \times [0,1]$. The initial conditions are discussed in the above reference. There are four shocks which divide the domain into four quadrants. The contact point in the original work is at (1/2, 1/2). We have shifted it to (3/4, 3/4), as in Serna (2006), for better visualization. In Figure 5 we show the numerical solution at t = 0.8 computed on a (1000 × 1000) grid with a CFL of 0.5. The basic structure is the same as has been computed by Serna [27] and Čada *et al.* [28], but the details of rolled-up structures indicate the enhanced accuracy of the present scheme. The second reference computed this case on the same grid with a TVD-MUSCL scheme - no small-sale roll-up was detected.

5.5 The four-contacts problem

This problem is also taken from Schulz-Rinne *et al.* [26]. The computational domain is a unit square. The nature of the solution is a clockwise turning vortex with four slip-lines spiralling around it. The result is shown in Figure 6, at t = 0.8. Comparing with Čada *et al.* [28], we note that the contacts are very well

resolved by COMPCS1 due to its high spectral accuracy. For this problem, schemes without adequate resolution fail to show any roll-up structure for the slip lines extending to the top right and bottom left quadrants. For the other two slip lines, a couple of small-scale vortices were displayed in Čada *et al.* [28]. The present solution, on the other hand, capture the small-scale vortices very well on all four slip lines.

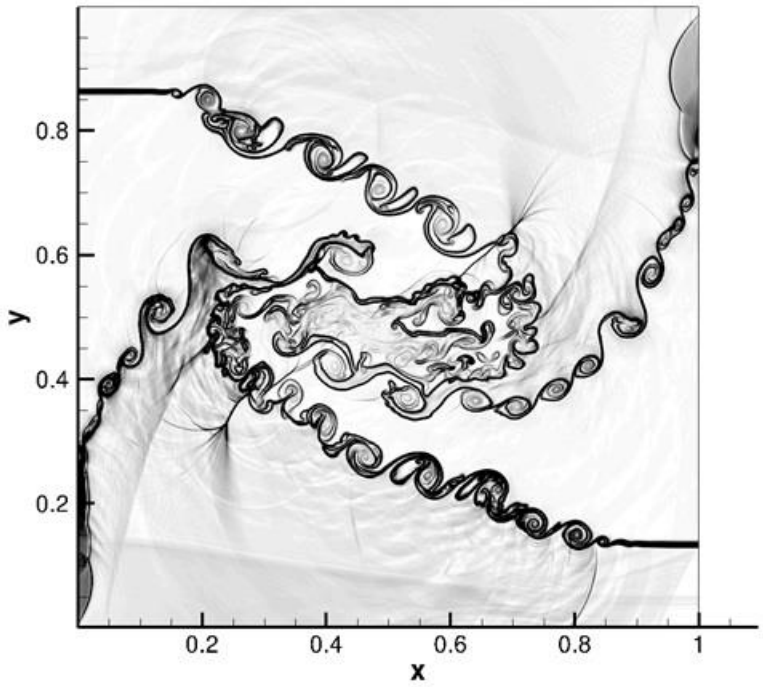

FIG 6. The four-contacts problem using the COMPCS1. Numerical schlieren at t = 0.8 with a CFL of 0.5. Grid size: 1000×1000; RK four-stage time stepping. Forty contours from 1 to 40 have been plotted.

6. Conclusion

We have presented a method of using a central compact scheme in a conservative manner in an Euler solver based on the AUSM$^+$ algorithm. No filtering, high order dissipation or any localized artificial diffusivity have been used. A TVD limiter invokes lower order dissipative formulae to stabilize the solution near discontinuities. In the smooth regions of the flow field the solver runs without any high-order dissipation. The key advantage of the present formulation is its low overall dissipation - which originates only from low-order formulae activated by the limiter at sharp gradients. The presented test cases confirm the adequacy of the limiter in handling shocks, and the high spectral accuracy and low dissipation of the overall scheme has been confirmed through small-scale roll-up structures in three two-dimensional standard configurations.

REFERENCES

[1] A.I. Tolstykh, World Scientific Publishing Co. Pvt. Ltd, 1994.
[2] A.I. Tolstykh, Dokl. Akad. Nauk SSSR, vol. 210(1), 1973, pp 48-51.
[3] R.S. Hirsh, J. Comput. Phys., vol. 19, 1975, pp 90-109.
[4] S.K. Lele, J. Comput. Phys., vol. 103, 1992, pp 16-42.
[5] A. Jameson et al., AIAA-Paper., vol. 1259, 1981.
[6] T.K. Sengupta et al., Comput. Fluids., vol. 88, 2013, pp 19-37.
[7] M.R. Visbal et al., J. Comput. Phys., vol. 181, 2002, pp 155-185.
[8] D.P. Rizetta et al., Prog. Aerosp. Sciences, vol. 44, 2008, pp 397-426.
[9] S. Kawai et al., J. Comput. Phys., vol. 229, 2010, pp 1739-1762.
[10] S. Pirozzoli, J. Comput. Phys., vol. 178, 2002, pp 81-117.
[11] Y.-X. Ren et al., J. Comput. Phys., vol. 192, 2003, pp 365-386.
[12] Tu.Guo. -Hua et al., J. Comput. Phys., vol. 225, 2007, pp 2083-2097.
[13] K.S. Ravichandran, Int. J. Comput. Fluid Dyn., vol. 8, 1997, pp 311-316.
[14] H. Jun et al., Int. J. Numer. Methods Fluids, vol. 56, 2008, pp 2139-2150.
[15] K.S. Ravichandran, Int. J. Comput. Fluid Dyn., vol. 3, 1994, pp 141-152.
[16] T.K. Sengupta et al., J. Comput. Phys., vol. 192, 2003, pp 677-694.
[17] M.-S. Liou, J. Comput. Phys., vol. 129, 1996, pp 364-382.
[18] R. Radespiel et al., J. Comput. Phys., vol. 121, 1995, pp 66-78.
[19] S. De et al., Int. J. Comput. Fluid Dyn., vol. 25(6), 2011, pp 345-354.
[20] K. H. Kim et al., J. Comput. Phys., vol. 208, 2005, pp 570-615.
[21] P.K. Sweby, SIAM J. Numer. Anal., vol. 21(5), 1984, pp 995-1011.
[22] M.H. Carpenter et al., NASA TM., vol. 109112, 1994.
[23] R. Artebrant et al., SIAM J. Scientific Comput., vol. 28(1), 2006, pp 359-381.
[24] S.-M. Chang et al., Shock Waves, vol. 10, 2000, pp 333-343.
[25] P. Halder et al., Shock Waves, vol. 23, 2013, pp 495-504.
[26] C.W. Schulz-Rinne et al., SIAM J. Scientific Comput., vol. 14(6), 1993, pp 1394-1414.
[27] S. Serna, SIAM J. Scientific Comput., vol. 28(1), 2006, pp 123-140.
[28] M. Čada, et al., J. Comput. Phys., vol. 228, 2009, pp 4118-4145.